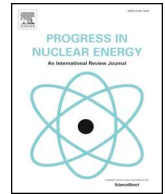




ELSEVIER

Contents lists available at ScienceDirect

Progress in Nuclear Energy

journal homepage: www.elsevier.com/locate/pnucene

Study on background shielding for a compact photoneutron source

X.H. Wang^{a,b,c}, L.X. Liu^{a,b}, J.F. Hu^{a,b}, J.L. Han^{a,b}, P. Yang^{a,b,c}, G.L. Zhang^{a,b}, N.X. Wang^{a,b,c}, X.Z. Cai^{a,b,c}, H.W. Wang^{a,c,*}, J.G. Chen^{a,b,c,**}^a Shanghai Institute of Applied Physics, Chinese Academy of Sciences, Shanghai, 201800, China^b CAS Innovative Academies in TMSR Energy System, Chinese Academy of Sciences, Shanghai, 201800, China^c University of Chinese Academy of Sciences, Beijing, 100049, China

ARTICLE INFO

Keywords:

TMSR
Compact photoneutron source
Subsection method
Variance reduction techniques

ABSTRACT

A compact photoneutron source (PNS), based on an electron LINAC was designed and constructed to provide required experimental nuclear data for Thorium Molten Salt Reactor (TMSR). All devices including the LINAC, the neutron production target and the detector systems were arranged in a shared hall, leading to a high background of neutron and γ -ray. The necessary shielding design was made to reduce the backgrounds. A series of preliminary measurements of total cross section in thermal neutron energy region for some key nuclides of TMSR, such as ^{232}Th and ^7Li , have been performed at this PNS. It was found, however, that additional shielding needs to be constructed to further reduce the neutron and γ -ray backgrounds. MCNP is a major tool for the background shielding design since it has the calculation capability for a coupled neutron-photon-electron transport problem. A two-step subsection simulation based on MCNP involving with variance reduction techniques (Sub-Var method) was performed to provide required flux and spectrum calculation for the new background shielding design. Based on the simulated results, a new local shielding was designed and constructed, which can reduce the thermal neutron background by three orders of magnitude and the γ -ray background by two orders of magnitude. The neutron flux and energy spectrum were measured under the new shielding condition and compared with the simulated ones, showing a good agreement with each other in the thermal energy region. Therefore, a significant improved shielding for the PNS is achieved, which is expected to provide a required assurance for the future measurements of neutron cross section at the PNS.

1. Introduction

The target accuracy of effective neutron multiplication factor uncertainty from nuclear data for the generation IV nuclear energy systems is estimated to reach about 0.3% which, of course, cannot be fulfilled by the existing nuclear data (Koning et al., 2009). Many electron accelerator-driven neutron sources, such as GELINA (Cocceva et al., 2002), nELBE (Klug et al., 2007) and PNF (Kim et al., 2002), were built to improve the accuracy of nuclear data for the design of advanced nuclear power reactors. In order to meet the requirements of nuclear data for Thorium Molten Salt Reactor (TMSR) (Jiang et al., 2012), a photoneutron source (PNS) driven by a 15 MeV electron LINAC has been built at Shanghai Institute of Applied Physics (SINAP) (Wang et al., 2014). The main objective of the PNS is to provide required neutron cross section measurements for some key nuclides concerning TMSR. Besides, benchmarking for evaluated nuclear data and validation for nuclear design codes are also expected to be performed at this

facility.

The PNS is a compact electron accelerator-driven neutron source which consists of an electron accelerator, a photoneutron target and a detector system. All these systems are arranged in an experimental hall with the space of 11 m \times 8 m, inevitably causing high backgrounds of neutron and γ -ray in the hall (Wang et al., 2014). For reducing the neutron and γ -ray backgrounds, a photoneutron target chamber made of aluminum, lead and polyethylene was constructed to prevent the neutrons and γ rays produced by the photoneutron target from scattering into the hall and a shielding box made of 10-cm thick boron polyethylene (PE-B, 5 wt% B) surrounding the neutron detector was applied to reduce the impact of backgrounds on the detector. Nevertheless, the experiments during the commissioning identified that the existing shields could not meet the requirements of cross section measurements. Therefore, a new shielding should be reconsidered to improve the measurements at the PNS, which must be able to depress significantly the background from neutrons and γ rays. It requires a

* Corresponding author. Shanghai Institute of Applied Physics, Chinese Academy of Sciences, Shanghai, 201800, China.

** Corresponding author. Shanghai Institute of Applied Physics, Chinese Academy of Sciences, Shanghai, 201800, China.

E-mail addresses: wanghongwei@sinap.ac.cn (H.W. Wang), chenjg@sinap.ac.cn (J.G. Chen).<https://doi.org/10.1016/j.pnucene.2019.03.026>

Received 2 April 2018; Received in revised form 7 December 2018; Accepted 17 March 2019

Available online 26 March 2019

0149-1970/ © 2019 Elsevier Ltd. All rights reserved.

multi-region shielding arrangement in the experimental hall by considering various factors causing the above backgrounds.

The local shielding design needs to get an accurate estimation of the flux and energy spectrum for interested particles at the measuring area. Monte Carlo method is extensively employed for shielding analysis of nuclear devices (Kirk, 2010). However, for a deep penetration problem occurring in the PNS, the direct analog Monte Carlo method calculates the actual transport course of various particles without considering the required variance reduction techniques, which is inefficient since the coupled neutron-photon-electron transport calculation for a complex geometry needs a large amount of computing time. Furthermore, neutrons would have little contribution to the signal recorded by a detector in a far-source region, thus a poor accurate result would be obtained if only a direct analog Monte Carlo method is adopted in the simulation (Sahiner et al., 2017). Finally, the electron beam losses in the accelerator tube, especially at the bending section have a great impact on the background levels, which must be reconsidered carefully in the new shielding design. All the above factors would lead to unreliable flux and energy spectrum estimations with unbearable computing time, if a conventional MCNP simulation is adopted.

Variance reduction techniques are applied extensively in the simulations for deep penetration problems, because it can reduce computing time and decrease statistic error significantly compared with the direct analog Monte Carlo method. It is important to choose appropriate variance reduction techniques for different deep penetration problems. For the PNS, the Geometry Splitting & Russian Roulette, DXTRAN sphere and forced collision techniques (Kiedrowski, 2012) were together used for the background shielding design. Furthermore, MCNP has the function to record all the neutrons and γ rays produced from the target by photonuclear reactions triggered by the LINAC electrons, and then to generate a surface source file. This generated source file can be utilized in the subsequent simulation for particle transport (Zhong and Gohar, 2011). Therefore, considering the possible re-estimation of background for different local shields, a subsection method was applied to reduce the computing time, which has also been used in the simulation of n_TOF at CERN (Borcea et al., 2003). This method together with the variance reduction techniques (Sub-Var method) divides the simulation into two steps. First, the SSW function of MCNP was utilized to record the neutrons and γ rays passing through a source window to generate the source file by a direct calculation. Second, the variance reduction techniques were adopted to reduce the computing time and the statistics error; and the SSR function of MCNP was utilized to read the generated source file in the first step for the subsequent calculation, which can also save much computational time due to the avoidance of repeated transport calculation of electrons. Finally, the measured neutron flux and energy spectrum at the PNS with the new shielding, were compared with the simulated ones to prove the reliability of the Sub-Var method and the validation of the new local shielding design.

This paper introduces a precise simulation method and demonstrates its application in the background shielding design and the flux and energy spectrum calculation for the PNS. The description of the PNS facility and its background is given in Section 2. Section 3 presents the introduction to the simulation model and method. A detailed discussion on the simulated results and verification is presented in Section 4.

2. Photoneutron source and its background

2.1. PNS facility

The experimental arrangement of the PNS is shown in Fig. 1. The PNS is driven by an electron LINAC which produces electrons with an adjustable operation mode characterized by 15–18 MeV average energy, 1.5–3 μ s pulse width, 10–260 Hz repetition rate. The maximum current is 0.1 mA and the maximum electron beam power on the photoneutron target is 1.5 kW. The electron beam hits the photoneutron

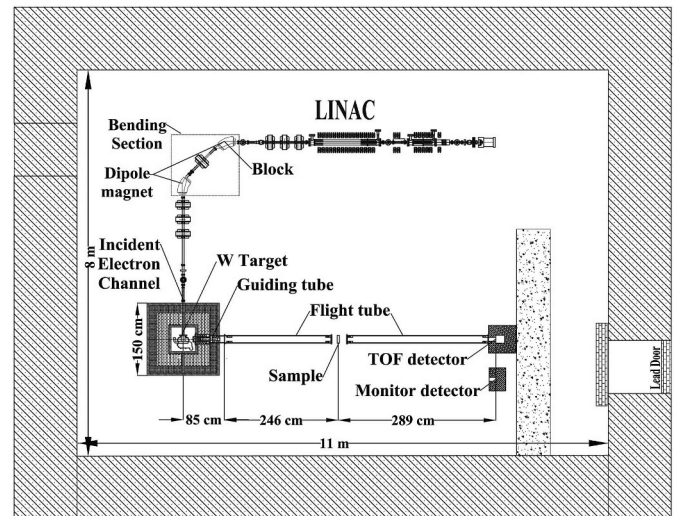


Fig. 1. Schematic view of the PNS.

target to produce the γ rays by the bremsstrahlung process. Then neutrons are produced by the secondary photoneutron reactions of γ rays in the photoneutron target.

A cylindrical tungsten target is adopted for the photoneutron production, which is 60 mm in diameter and 48 mm in thickness with a purity of 98%. It is placed at the center of the target chamber and welded on a water-cooled copper pedestal. In order to reduce the neutron and γ -ray backgrounds, the photoneutron target is shielded by a box consisting of 5-cm aluminum, 25-cm lead, 15-cm polyethylene and 5-cm aluminum, in sequence. The neutron guiding tube is aligned vertically to the electron beam while the γ rays guiding tube is aligned with the electron beam forward direction, which is blocked by a lead plate at present. Neutrons from the target go through a lead plate with a thickness of 5 cm for reducing the impact of γ rays, followed by a 10-cm thick polyethylene plate to slow down the fast neutrons. The diameter of neutron beam is then collimated from 10 cm to 5 cm by a PE-B tube and a lead tube.

After coming out from the guiding tube, the neutrons fly to the detector through two stainless steel tubes with the same diameter of 14 cm and two different lengths, 246 cm and 289 cm. At both ends of each tube, two collimators, composed of lead and PE-B block with the same inner diameter and thickness of 5 cm, are installed to provide an additional collimation for the neutron beam. Between the two tubes, a 30 cm space is reserved for the arrangement and change of sample targets. The total neutron flight path is 6.2 m.

Two identical neutron detectors are used in the experiments. A detector is located at the end of the second neutron guiding tube, which is used to detect the transmitted neutrons from the photoneutron target as a TOF detector. The other is placed at the lower left of the first detector for monitoring the neutron intensity.

2.2. Neutron background

It is crucial to identify all key source terms causing backgrounds from various components of the PNS and provide the required information for the new shielding design. According to the accelerator design analysis and the measurements of the radiation dose in the hall and outside of the building, the neutron background arises primarily from three aspects.

The first one is from the electron beam loss at the accelerator bending section which is shown in Fig. 1. When the electrons are accelerated to the rated energy, the electron beam is deflected in 90° by two dipole magnets due to the hall space constraint. Three beam blocks are used to sweep away the undesired electrons with energies beyond

the designated range, while one of them is for removing high energy electrons and the other two are for removing low energy electrons. These lost electrons would react with surrounding materials and then generate neutrons and γ rays. The loss ratio of the electron beam is about 30%.

The second one is the back forward neutrons relative to the incident electron direction from the photoneutron target chamber. The electron beam tube is directly connected to the target without any blocking materials, thus part of the neutrons produced by the tungsten target would fly out from this tube causing a scattering background in the experimental hall.

The third one is from the neutron loss caused by the collimation in the flight path. When coming out from the guiding tube, the neutron beam is not rigorously in parallel. The collimators are thus needed to control the diameter of the neutron beam in 5 cm. The neutrons which are blocked by the collimators would be scattered to the experimental hall. In addition, the fast neutrons that pass through the collimators would also have effects on the TOF detector.

3. Simulation model and method

3.1. Shielding geometry

Accurate modeling is also crucial for obtaining reliable simulated flux and energy spectrum and optimizing the shielding design of the PNS. The MCNP geometry for this problem was simulated in two parts for the facility and its local shields. The model of facility was simulated in detail, as described in Section 2.1. The model of local shields is shown in Fig. 2.

The ultimate objective of the new shielding design is to reduce the thermal neutron background. The material used in the shielding must be able to absorb or block the electrons, γ rays and neutrons without producing the new backgrounds. Therefore, three local shields were arranged by comprehensively considering different kinds of factors, such as sources of background, space limitation and the bearing capacity of foundation of the experimental hall.

First, in order to avoid the lost electrons at the accelerator bending section reacting with the surrounding materials to produce the new neutron and γ -ray backgrounds, an aluminum plate, which has the lower bremsstrahlung yield and can be less easily activated than other materials such as iron and lead (Patil and Dhole, 2010), was used to block the lost electrons. Then, a lead plate was taken to shield the γ rays produced in bremsstrahlung process, and a PE-B plate which has great neutron shielding performance was placed on the outside of the lead

plate to block the neutrons produced by photoneutron reactions. Thus, a shield (named S1) composed of an aluminum plate with thickness of 5 cm, a lead plate with thickness of 15 cm and a PE-B plate with thickness of 10 cm in sequence, was used to block the neutrons and γ rays produced from the accelerator bending section and to reduce the radiation dose outside of the building.

Second, the backgrounds in the experimental hall are so high, that it is necessary to separate the detector system from the other systems for further reducing the influence of backgrounds on the detector. Thus, an L-type shielding wall (named S2) made of concrete and PE-B with thickness of 30 cm and height of 200 cm was arranged to surround the detector system in the experimental hall. The PE-B wall was placed on the side near the detector system. This shielding wall can prevent the neutrons and γ rays produced in the accelerator bending section and the target chamber leakage from entering the detector.

Third, a shielding box (named S3) with dimension of $100 \times 100 \times 100 \text{ cm}^3$ was constructed to surround the TOF detector. This box is made of 30 cm thick PE-B which can shield the thermal neutrons that cannot be blocked by the L-type shield. Therefore, this shielding box provides an additional protection for the detector.

Since the beam loss at the bending section is up to 30%, the background source term at the bending section should not be ignored. Therefore, two electron surface sources were used in the direct simulation, as shown in Fig. 2. One was placed at surface A to generate the electrons to hit the photoneutron target. The other was placed at surface B for analyzing the influence of electron beam loss at the bending section. The diameters of the two surface sources are both 5 mm, and their relative intensity of source are 0.7 and 0.3, respectively.

3.2. Variance reduction methods

As mentioned above, the simulation for the geometry of the PNS for shielding design by a direct calculation is a very difficult and time-consuming task. The solid angle of the TOF detector to the neutron source is so small that very few neutrons can be scored by the detector. Fortunately, the extensively used variance reduction techniques can sample more particles in the interesting region than the direct analog Monte Carlo calculation method. Thus, the statistical error in the simulation can be reduced significantly, and more accurate results can be obtained. There are many variance reduction techniques, and it is therefore necessary to choose suitable variance reduction techniques for the PNS.

Three variance reduction techniques, including Geometry Splitting & Russian Roulette, DXTRAN sphere and forced collision, were applied to increase the simulation performance for the PNS.

First, the Geometry Splitting & Russian Roulette controlled by IMP card is helpful for the particles moving more easily to the important regions of the PNS (Polo et al., 2017). Of which, the most important region is the path interval from the photoneutron target to the detector, where 12 cells were designated with different importance. When the particles of weight w move from a cell with importance I_1 to another cell with importance I_2 ($I_2 > I_1$ and I_2/I_1 is an integer n ($n \geq 2$)), they are split into n identical particles with each weight w/n , to provide a better sampling. When the particles move to a cell with a less importance I_3 , the Russian Roulette is employed, and the particles are killed with the probability $1-(I_3/I_1)$ or followed with the probability I_3/I_1 and the weight $w^* I_3/I_1$, to avoid wasting computing time.

Then, as one of the most useful techniques in the simulation of streaming problems, the DXTRAN sphere was used to force particles to a small region of space that they will be otherwise very unlikely to go (Kiedrowski, 2012). DXTRAN sphere is an artificial sphere containing a tally cell, thus the angular biasing is performed to pull particles toward this sphere. The inner sphere must cover the detector cell and the outer sphere should surround the neighboring regions whereby the neutrons may be scattered into the detector. The weight cutoff parameters are used for ensuring that the computing time is not wasted on the

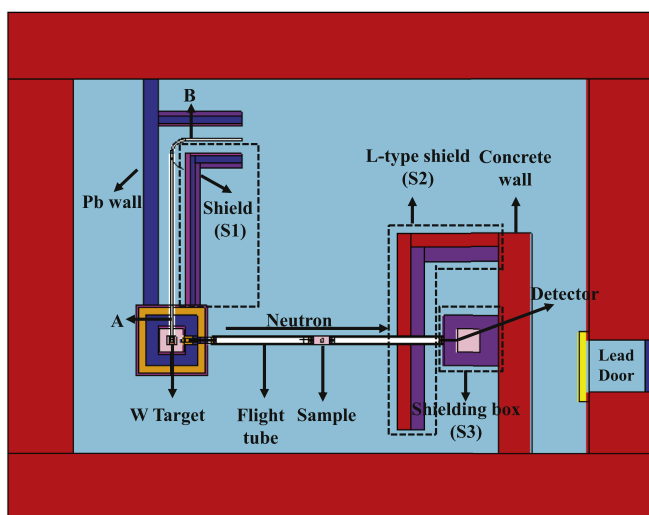


Fig. 2. Schematic model for the simulation of the PNS.

simulation of particles with very low weight.

Last but not least, because detector counts and DXTRAN particles arise only from collisions and source, the forced collision method controlled by FCL card, was used in some cells to increase the number of collisions that can produce large detector counts and large weight DXTRAN particles (X-5 Monte Carlo Team, 2004). It splits particles into an uncollided part and a collided part. The uncollided part immediately exits the current cell without collision and transport continues. The collided part is forced to collide within the current cell, and the weight is partitioned according to the probability of colliding.

3.3. Sub-Var method

Although the variance reduction techniques can reduce the computing time and decrease the statistic error, it would still take much time to complete the whole simulation due to the coupled electron-neutron-photon transport for the complex PNS geometry. The SSW function in MCNP can record the neutrons and γ rays passing through a specific surface or cell to generate a source file which can then be read by the SSR function to carry out the subsequent simulation. Hence, the simulation process can be separated into two steps, which is called subsection.

In the first step, assuming that the new local shields can block most of the neutron and γ -ray backgrounds, it can be said that the electron beam loss at the bending section has a very limited impact on the background, and thus this background source term was no longer considered in the simulation. Only one electron surface source at surface A was applied to generate electrons. A direct calculation with the detailed geometry was performed by MCNP. The source window was constructed at the center of target chamber which is composed of six surfaces. Four of the six surfaces (A, B, C and D) are shown in Fig. 3 (surfaces E and F are not shown for simplicity). All the produced neutrons and γ rays passing through the window were recorded into a WSSA file by the SSW function. The advantage of this setup is that this source file can be utilized many times by repeated simulations without changing the source window.

In the second step, the generated source file in the first step was used to perform an independent simulation of the PNS without needing to consider the electrons, which can save much time for the iterative

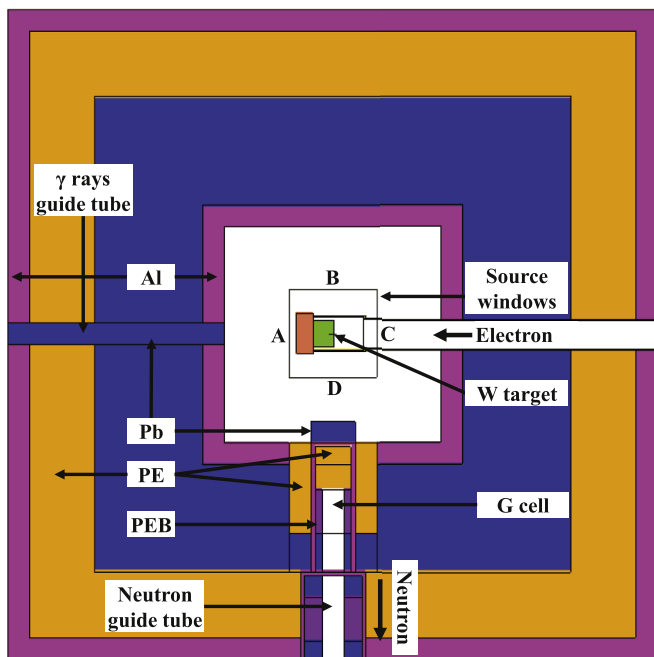


Fig. 3. Simulating graph of the target chamber.

optimization of shielding design for the PNS. All the neutrons and γ rays that reenter the source window were killed to prevent the neutrons from the window being recounted, which thus avoids the undesired overestimated results. The Geometry Splitting & Russian Roulette, DXTRAN sphere and forced collision mentioned in section 3.2 were applied to obtain the results with sufficient precision.

For the direct simulation, the NPS which means how many particles to run was set to 5×10^8 . For the Sub-Var method in the second step, the NPS was set to 2×10^9 which is helpful to reduce the calculation error. If the NPS of direct simulation was also set to 2×10^9 , the computing time is nearly about a month which is unbearable to the PNS shielding design. The calculation were carried out in the TMSR Supercomputing Center while 12 processors were employed for the direct calculation and only two processors were applied for the Sub-Var method since the generated source file was too large to take more processors for the parallel computing. Both the neutron data and photonuclear data were from ENDF/B-VII.0 (X-5 Monte Carlo Team, 2004). Considering the impact of thermal neutron scattering effect of the polyethylene, $S(\alpha, \beta)$ from ENDF/B-VII.0. was taken (Borcea et al., 2003).

4. Results and discussion

4.1. Shielding effects

In order to verify the accuracy of the shielding design simulation, the neutron background at the TOF detector was calculated by the variance reduction methods. A PE-B cube with a length of 12.8 cm was placed at the sample target area to block the neutrons from the photoneutron target for background measurement, as discussed in Ref. (Liu et al., 2017). To study the shielding performance, six different shielding configurations are discussed. The result is shown in Fig. 4, where S0 represents that no shields are used in the simulation, S2/S3 represents that both L-type shield and the shielding box are used, S1/S2/S3 represents that all shields are used in the simulation.

By comparing the results of S0, S1, S2, S3 and S1/S2/S3, one can find that the shielding box (S3) surrounding the TOF detector has the strongest neutron shielding ability, which can reduce the neutron background by two orders of magnitude. When all the shields are applied (S1/S2/S3), the neutron background is reduced by nearly three orders of magnitude. Although the PE-B cube can not block the γ rays from the photoneutron target for the background measurement, it can still be seen from Fig. 4, that the γ -ray background is reduced by two orders of magnitude. Thus, it is indicated that the new local shields are effective.

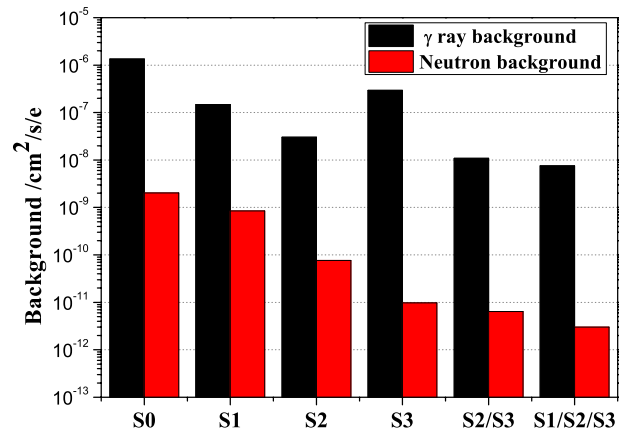


Fig. 4. Simulated backgrounds of neutron and γ -ray under various shields. (S0: No shields; S1: Shield at the bending section; S2: L-type shield; S3: Shielding-box; S2/S3: Shields include S2 and S3; S1/S2/S3: All shields include S1, S2 and S3.)

When all the shields are applied (S1/S2/S3), the neutron and γ -ray backgrounds are about half of that obtained with the L-type shield and the shielding box (S2/S3). It means that the S2/S3 shields block most of the background neutrons and γ rays and the contribution of S1 shield is relatively small. Therefore, when S2/S3 shields are applied, the background source term at the bending section needs not be considered in the first step of the Sub-Var method for further reducing the computing time.

4.2. Neutron flux and energy spectrum

To verify the reliability of the Sub-Var method and the validation of the new shielding, the neutron flux and energy spectrum at the TOF detector area were measured under the new shielding condition. The electron energy was 16 MeV and the electron beam power on the photoneutron target was 1050 W during the operation. Three sample targets were used for cycle testing and a measured time of 300 s was set for each sample. The first one was a set of notch filters containing Cd, Co, Ag and In for neutron energy calibration. The second one was a PE-B cube with a length of 12.8 cm to block the neutrons from the photoneutron target for background measurement. The last one was an open target which is a blank sample. The $^6\text{LiF}(\text{ZnS})$ scintillator with the product code of EJ426HD2 was used for neutron TOF measurement due to its high detection efficiency for thermal neutrons but with low sensitivity to γ rays radiation. The neutron flux and energy spectrum can be obtained with the TOF technique. The DAQ system used in the experiments was described in detail in Ref. (Liu et al., 2016).

First of all, it is important to check the reliability of the source file which was generated by the SSW function through the direct calculation. Due to the difficulty in scoring enough counts at the TOF detector area by the direct calculation, as mentioned above, the flux and energy spectrum of neutrons and γ rays at G cell (behind the polyethylene plate, as shown in Fig. 3) were calculated by the direct calculation method and the Sub-Var method to verify the source file. The results are shown in Table 1 and Fig. 5. It is found that the two methods give the almost same flux and energy spectrum. Therefore, it is concluded that the function of MCNP have been implemented correctly in the Sub-Var method and the source file generated in the first step can be used for the subsequent calculation.

Then, the source file was used in the second step of the Sub-Var method for the simulation of neutron flux and energy spectrum at the TOF detector. The detection efficiency of the detector has been considered in all the calculations. The results are shown in Table 2 and Fig. 6.

Table 2 shows that the calculated neutron flux by the direct calculation method is $168.1/\text{cm}^2/\text{s}$ in the energy region from 0.001 eV to 100 eV, and the computing time is up to 168 h with a relative error of 99.95%. The calculated neutron background is 0 which means that the calculated result is invalid. When the Sub-Var method is adopted, the simulated neutron flux is $83.4/\text{cm}^2/\text{s}$ which is 20% larger than the measured result. The simulated result passes all statistical checks which is helpful to guarantee the reliability of the simulation (X-5 Monte Carlo Team, 2004). The figure of merit (FOM) which means the efficiency of the calculation is increased from 10^{-5} for the direct calculation to 4.3 for the Sub-Var method. And the relative error is reduced from 99.95% to 1.6%. Meanwhile, the computing time for the latter is reduced to 35 h, nearly five times of simulation efficiency higher than the former. The simulated neutron background is about $0.8/\text{cm}^2/\text{s}$ which is a half of

Table 1
Simulated results of neutron and γ -ray flux at G cell by direct calculation and Sub-Var method.

	Neutron flux ($/\text{cm}^2/\text{s}/\text{e}$)	Gamma flux ($/\text{cm}^2/\text{s}/\text{e}$)
Direct Calculation	$4.947 \times 10^{-8} \pm 0.0118$	$1.097 \times 10^{-5} \pm 0.0055$
Sub-Var Method	$4.987 \times 10^{-8} \pm 0.0062$	$1.046 \times 10^{-5} \pm 0.0014$

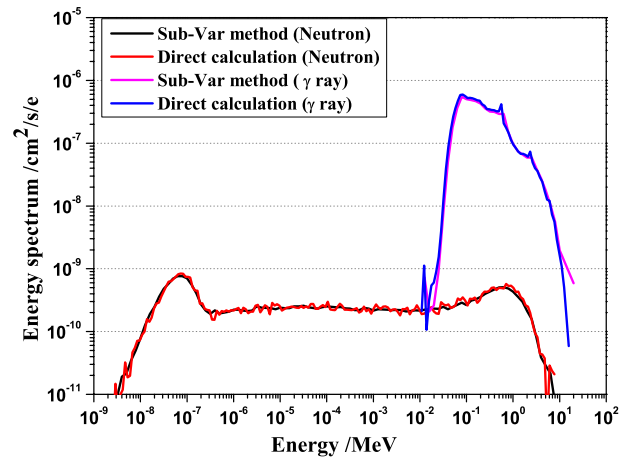


Fig. 5. Calculated energy spectrum by direction calculation and Sub-Var method.

Table 2
Simulated neutron flux and background in the thermal energy region and the corresponding relative errors, FOM, computing time and the experimental data.

		Results ($/\text{cm}^2/\text{s}$)	Relative Error (%)	FOM	Time(h)
Direct Calculation	Neutron flux	168.1	99.95	10^{-5}	168
	Background	0.0	0.0	0.0	150
Sub-Var method	Neutron flux	83.4	1.6	4.3	35
	Background	0.8	15.5	0.018	37
Measured results	Neutron flux	69.3	5.0	–	0.25
	Background	1.6	5.0	–	0.25

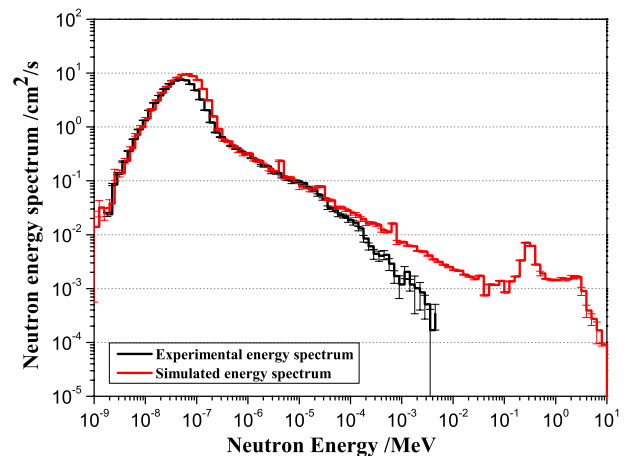


Fig. 6. Simulated and measured neutron spectrum at the TOF detector.

the measured background, due to the fact that the influence of electron loss at the bending section was not considered in the simulation. As a whole, the simulated neutron flux shows a good agreement with the measured result, namely, the neutron background is reduced to an acceptable range.

When computing the neutron spectrum, the influence of neutron background is removed by killing the neutrons which touch the collimators or the tubes. The simulated neutron energy spectrum is shown in Fig. 6 and compared with the measured one. It is observed that the energy spectrum of the PNS presents a wide energy region, from 0.001 eV to 10 keV. In the energy range from 0.001 eV to 100 eV, the simulated result shows a good agreement with the measured one. The slight discrepancy in this energy range is caused by the difference of the moderator parameters such as density and composition between the

simulation and measurement. Above 100 eV, the deviation between the simulated result and the measured one gradually increases. Due to the application of the pulse-shape discrimination (PSD) method for the n/γ identification of TOF spectrum, there is a threshold for time of flight of neutrons. Thus, the fast neutrons arriving time signal near the big gamma flash pulse cause a long dead time (Liu et al., 2016, 2017), which makes the measured neutron counting by the detector lower than the actual one. In addition, the detection efficiency of the detector in this energy region is less than 1%, which has a great influence on the neutron counting. Accordingly, it can be concluded that the discrepancy between the simulation and measurement is acceptable.

5. Conclusions

In this work, a subsection method combining with variance reduction techniques based on MCNP was introduced to increase the simulation efficiency and accuracy for the background shielding design of the PNS. The simulation process was divided into two steps. First, the electron transport calculation was performed once to generate a source file containing the neutrons and γ rays information. Second, the source file was utilized for the subsequent MCNP calculation without wasting time on the electrons transporting, and the variance reduction techniques including Geometry Splitting & Russian Roulette, DXTRAN sphere and forced collision were taken to reduce the uncertainties in the simulations. Based on the above simulations, local shielding in the PNS hall was updated. It indicates that the new shielding design can reduce by three orders of magnitude for the neutron background and by two orders of magnitude for the γ -ray background. The calculation efficiency is increased by nearly 5 times than that with the direct analog Monte Carlo calculation method, and the relative error is reduced to 1.6%. Both the simulated neutron flux and energy spectrum at TOF detector area show a good agreement with the experimental ones. It is concluded that the Sub-Var method has a high capacity to model the PNS effectively and can provide accurate simulated neutron flux and energy spectrum. The new local shielding design guided by the simulation results can reduce the neutron and γ -ray backgrounds to an acceptable range, therefore paving the way for the neutron physical experiments at the PNS in the future.

Acknowledgments

This work is supported by the Chinese TMSR Strategic Pioneer Science and Technology Project under Grant No. XDA02010000, the National Natural Science Foundation of China under Grant No. 11475245, 91326201 and the Frontier Science Key Program of the Chinese Academy of Sciences under Grant No. QYZDY-SSW-JSC016.

Appendix A. Supplementary data

Supplementary data to this article can be found online at <https://doi.org/10.1016/j.pnucene.2019.03.026>.

References

- Borcea, C., Cennini, P., Dahlfors, M., Ferrari, A., Garcia-Muñoz, G., Haefner, P., Herrera-Martínez, A., Kadi, Y., Lacoste, V., Radermacher, E., Saldaña, F., Vlachoudis, V., Zanini, L., Rubbia, C., Buono, S., Dangendorf, V., Nolte, R., Weiergan, M., 2003. Results from the commissioning of the n_TOF spallation neutron source at CERN. *Nucl. Instrum. Methods Phys. Res., Sect. A* 513 (3), 524–537.
- Coceva, C., Frisoni, M., Magnani, M., Mengoni, A., 2002. On the figure of merit in neutron time-of-flight measurements. *Nucl. Instrum. Methods Phys. Res., Sect. A* 489 (1), 346–356.
- Jiang, M.H., Xu, H.J., Dai, Z.M., 2012. Advanced fission energy program-TMSR nuclear energy system. *Bull. Chin. Acad. Sci.* 27, 366–374.
- Kiedrowski, B.C., 2012. MCNP6 for criticality accident alarm systems – a primer, Tech. Rep. LA-UR-12-25545. Los Alamos Natl. Lab. 24–27.
- Kim, G.N., Kovalchuk, V., Lee, Y.S., Skoy, V., Cho, M.H., Ko, I.S., Namkung, W., Lee, D.W., Kim, H.D., Ko, S.K., 2002. Measurement of photoneutron spectrum at pohang neutron facility. *Nucl. Instrum. Methods Phys. Res., Sect. A* 485 (3), 458–467.
- Kirk, B., 2010. Overview of Monte Carlo radiation transport codes. *Radiat. Meas.* 45 (10), 1318–1322.
- Klug, J., Altstadt, E., Beckert, C., Beyer, R., Freiesleben, H., Galindo, V., Grosse, E., Junghans, A., Légrády, D., Naumann, B., Noack, K., Rusev, G., Schilling, K., Schlenk, R., Schneider, S., Wagner, A., Weiss, F.-P., 2007. Development of a neutron time-of-flight source at the ELBE accelerator. *Nucl. Instrum. Methods Phys. Res., Sect. A* 577 (3), 641–653.
- Koning, A.J., Blomgren, J., Jacqmin, R., Plompen, A.J.M., Mills, R., Rimpault, G., Bauge, E., Ott, D.C., Czifrus, S., Dahlbacka, K., 2009. CANDIDE: Nuclear Data for Sustainable Nuclear Energy.
- Liu, L.X., Wang, H.W., Ma, Y.G., Cao, X.G., Cai, X.Z., Chen, J.G., Zhang, G.L., Han, J.L., Zhang, G.Q., Hu, J.F., Wang, X.H., 2016. Neutron time-of-flight spectroscopy measurement using a waveform digitizer. *Chin. Phys. C* 40 (5), 70–74.
- Liu, L.X., Wang, H.W., Ma, Y.G., Cao, X.G., Cai, X.Z., Chen, J.G., Zhang, G.L., Han, J.L., Zhang, G.Q., Hu, J.F., Wang, X.H., Li, W.J., Yan, Z., Fu, H.J., 2017. Measurements of the total cross section of natbe with thermal neutrons from a photo-neutron source. *Nucl. Instrum. Methods Phys. Res., Sect. B* 410, 158–163.
- Patil, B., Dhole, S., 2010. Studies on (i) Characterization of Bremsstrahlung Spectra from High Z Elements and (ii) Development of Neutron Source Using MeV Pulsed Electron Beam and Their Applications. Ph.D. thesis. University of Pune.
- Polo, I.O., Santos, W.S., de Lara Antonio, P., Caldas, L.V., 2017. Variance reduction technique in a beta radiation beam using an extrapolation chamber. *Appl. Radiat. Isot.* 128, 154–157.
- Sahiner, H., Norris, E.T., Bugis, A.A., Liu, X., 2017. Improved shielding design with an accelerated Monte Carlo simulation for a neutron generator at Missouri S&T. *Prog. Nucl. Energy* 97, 123–132.
- Wang, H.W., Chen, J.G., Cai, X.Z., Lin, Z.K., Ma, Y.G., Zhang, G.L., et al., 2014. Development of photo-neutron facility driven by electron LINAC. *Nucl. Tech.* 37, 114–118.
- X-5 Monte Carlo Team, 2004. MCNP-A General Monte Carlo N-Particle Transport Code, Version 5.
- Zhong, Z., Gohar, Y., 2011. Shielding design and analyses of KIPT neutron source facility. *Prog. Nucl. Energy* 53 (1), 92–99.